Energy Losses in Soft Magnetic Materials Under Symmetric and Asymmetric Induction Waveforms

Energy Losses in Soft Magnetic Materials under Symmetric and Asymmetric Induction Waveforms

Hanyu Zhao, Carlo Ragusa, Carlo Appino, Olivier de la Barrière,
Youhua Wang, and Fausto Fiorillo

***Abstract*— Magnetic losses under triangular symmetric and asymmetric induction waveforms have been measured over a broad range of frequencies and predicted starting from standard results obtained with sinusoidal induction. Non-oriented Fe-Si and Fe-Co sheets, nanocrystalline Finemet–type ribbons, and Mn-Zn ferrites have been investigated up to f = 1 MHz and duty cycles ranging between 0.5 and 0.1. The intrinsic shortcomings of the popular approach to loss calculation of inductive components in power electronics, based on the empirical Steinmetz equation and its numerous modified versions, are overcome by generalized application of the Statistical Theory of Losses and the related concept of loss separation. While showing that this concept applies both to ferrites and metallic alloys and extracting the hysteresis (quasi-static), excess, and classical loss components, we relate in a simple way the magnetic energy losses under symmetric triangular induction (square wave voltage) and sinusoidal induction. The loss behavior under asymmetric triangular induction is retrieved from the symmetric one, by averaging the energy losses pertaining to the two different semi-periods. Good comparison with the experimentally measured energy loss versus frequency behavior is demonstrated in all materials.**

***Index Terms*—Magnetic Losses, Inductors, Soft Magnetic Materials, Skin effect, Loss measurements.**

I. Introduction

Non-sinusoidal voltage waveforms are ubiquitously found in magnetic components employed in power electronics. Besides the distortion engendered by the non-linear response of the material, a variety of pulsed and rectangular voltages are imposed in electrical machine cores and in various types of inductive devices. In order to find the magnetic components and the design providing the best tradeoff between costs and performance, a method to predict the magnetic losses for realistic working conditions should therefore be devised. A case in point is one of symmetric and asymmetric triangular-trapezoidal induction waveforms, a typical regime imposed to the inductive components found in Switch Mode Power Supplies, converters, and permanent magnet motors. The buck DC-DC converter working in continuous mode provides a fitting example [1]. This is a standard device used to supply a load R_{load} with a DC voltage V_{out} lower than the input DC voltage V_{dc}, where the employed inductor is excited by an asymmetric sawtooth current.

This paper is devoted to measurement and analytical prediction of the magnetic losses in different materials on a broad frequency range, under symmetric and asymmetric triangular induction waveforms. Finding a way to calculate the magnetic losses under non-conventional operating modes starting from a minimum set of data, either measured directly or provided by the manufacturer, is an appealing objective, highly suitable for applications, where circuit designers still rely on empirical models. On the other hand, the broadband loss figures pertaining to such modes, namely the rectangular voltage waveforms, are much more difficult to achieve by measurements than in the usual case of sinusoidal voltage and are not available on the data sheets.

The standard approach of the literature is based on the Steinmetz equation and its many extended/improved versions, like the Modified Steinmetz Equation MSE [2], the Generalized Steinmetz Equation GSE [3], the Improved Generalized Steinmetz Equation iGSE [4], [5], the Natural Steinmetz equation NSE [6], and the Waveform Coefficient Steinmetz Equation WcSE [7]. The standard Steinmetz equation for the power loss under sinusoidal induction at given frequency f and peak value B_p, is expressed as $P = kf^{\alpha} B_p^{\beta}$, where k, α, and β are adjustable parameters. In order to deal with non-sinusoidal induction, it is modified in the iGSE according to the equation

$$P = f \int_0^{1/f} k_i \left|\frac{dB}{dt}\right|^{\alpha} (\Delta B)^{\beta-\alpha} dt \qquad (1)$$

for a peak-to-peak induction value ΔB. The parameter k_i is here a suitable combination of k, α, and β. This formulation aims at a more realistic account of the dependence, lumped in the exponent α, of the power loss on the induction derivative. However, despite the claimed successful comparison with the experiments, the empirical character of the Steinmetz approach is unsatisfactory from a scientific viewpoint and the source of practical limitations. The involved parameters are, for example, dependent on frequency and flux density [6] and the domain of application can be widened at the cost of an increasing number of pre-emptive measurements [8].

H. Zhao is with the State Key Laboratory of Reliability and Intelligence of Electrical Equipment and Key Laboratory of Electromagnetic Field, Hebei University of Technology, China, with Politecnico di Torino, Torino, Italy, and Istituto Nazionale di Ricerca Metrologica INRIM, Torino, Italy (hanyu.zhao@polito.it).

C. Appino and F. Fiorillo are with the Istituto Nazionale di Ricerca Metrologica INRIM, Torino, Italy (c.appino@inrim.it, f.fiorillo@inrim.it)

C. Ragusa is with Politecnico di Torino, Torino, Italy (carlo.ragusa@polito.it).

O. de la Barrière is with SATIE-ENS, UniverSud, Cachan, France (olivier.de-la-barriere@satie.ens-cachan.fr).

Y. Wang is with the State Key Laboratory of Reliability and Intelligence of Electrical Equipment and Key Laboratory of Electromagnetic Field, Hebei University of Technology, China (wangyi@hebut.edu.cn)

Corresponding author: Dr. Fausto Fiorillo, Istituto Nazionale di Ricerca Metrologica INRIM, Strada delle Cacce 91. 10135 Torino, Italy. Tel. +39 011 3919836; Fax: +39 011 3919834; e-mail: f.fiorillo@inrim.it

A certain difficulty in physically assessing the behavior of the magnetization process, its evolution with frequency and the related dissipation mechanisms [2] is one main reason for the persisting acceptance of the Steinmetz equation in the engineering milieu. Actually, the problem of predicting by analytical formulation the magnetic loss in soft magnetic sheets subjected to non-sinusoidal induction waveform has since long been posed, *in the absence of skin effect*, under the firm physical background offered by the Statistical Theory of Losses (STL) [9] and the related loss decomposition concept [10]. Trapezoidal and triangular induction waveforms have been treated in [11] and related applications have been reported, among others, in [12], [13], [14]. Further theoretical improvements, including loss prediction with minor loops, were obtained in [15] and pertaining concepts were later invoked in [16]. With the average energy loss at a given frequency $W(f) = P(f)/f$ composed of a frequency independent hysteresis (quasi-static) W_{hyst}, classical $W_{cl}(f) \propto f$, and excess $W_{exc}(f) \propto f^{1/2}$ contributions, according to $W(f) = W_{hyst} + W_{cl}(f) + W_{exc}(f)$, and with the instantaneous dynamic power loss values evolving in steel sheets as $P_{cl}(t) \propto (dB/dt)^2$ and $P_{exc}(t) \propto |dB/dt|^{3/2}$, the model can naturally incorporate the prediction for generic periodic $B(t)$. A recent application of this concept concerning the inductor loss (Sendust powder core) in a buck converter has been proposed, although on a restricted frequency range (40 kHz – 100 kHz) [17]. On the contrary, awkward adaptation of the Steinmetz parameters to any specific $B(t)$ law is imposed by the empirical character of the involved equations [8]. It is understood, for example, that defined single values for these parameters cannot comply with the obviously different frequency dependence of static and dynamic energy losses.

On the other hand, the STL-based model has been so far mostly applied for working regimes of electrotechnical interest, typically on steel sheets excited up to a few hundred Hz with symmetric $B(t)$ waveforms. With growing applications (e.g., in electric vehicles) of high-speed rotating machines and increasing working frequencies in power electronics, the need for broadband modeling of magnetic losses, including versatile treatment of non-sinusoidal regimes (e.g., triangular induction with symmetric/asymmetric duty cycles) has become apparent.

In this study, we investigate the energy loss versus frequency properties of thin (~ 0.20 mm) Fe-Si and Fe-Co steel sheets, measured up to a few kHz, of field-treated high-permeability nanocrystalline Finemet ribbons, and of Mn-Zn ferrite samples, up to the MHz range. Physical and geometrical parameters of the investigated samples are provided in Table I. Sinusoidal, triangular symmetric and triangular asymmetric induction waveforms have been considered, with duty cycle a ranging between 0.5 (symmetric wave) and 0.1. Starting from the $W(f)$ behavior measured under sinusoidal induction, we retrieve the associated loss components and transform them into the corresponding components for symmetric triangular induction. Remarkably, the method permits one to identify, on the one hand, the critical frequency for the appearance of the skin effect in the steel sheets (f_c ~ 800 Hz in Fe-Co and f_c ~ 1500 Hz in Fe-Si) and, on the other hand, to correspondingly manage the loss decomposition upon the whole investigated DC – 5 kHz range. At the same time, it is applied up to the MHz range in the nanocrystalline and ferrite samples. In this case, a generalized classical loss component $W_{cl}(f)$ is discussed and calculated. With the so predicted $W(f)$ for symmetric triangular induction, we can easily derive the $W(f)$ behavior for the asymmetric waveforms, combining the losses pertaining to the two different duty cycles, that is, the two different frequencies $f_1 = 1/(2aT)$ and $f_2 = 1/(2(1-a)T)$.

Such a broad combination of different materials and frequency ranges is, to authors' knowledge, unique. The fact that high frequencies are involved in applications has prompted many literature investigations at such frequencies, generally upon a narrow band [17]. However, comprehensive modeling calls for wideband measurements.

We remark that the role of the DC bias, like the one imposed by the load in a buck converter, is not considered in the present treatment, for the sake of simplicity. It could be considered, at least in the absence of deep skin effect, by a pure phenomenological approach [18] or with the method introduced in [19], leading to the prediction of the loss with sinusoidal induction and bias starting from the separation without bias (symmetric minor loops). This would require, however, the introduction of a hysteresis model (e.g., the Preisach model) and numerical calculations and would be at odds with our declared aim of developing a simple analytical approach. The presently discussed method can actually provide substantial prediction of the loss under square-wave voltage, even in the presence of a DC bias, if one can obtain this figure via the much simpler measurements under sinusoidal voltage. In such a case, we can again perform the loss separation, because the classical loss $W_{cl}(f)$ is independent of the bias, and simply retrieve the loss components for square-wave voltage. This will be further discussed in the following.

TABLE I

PHYSICAL PARAMETERS OF THE INVESTIGATED MATERIALS

Material	NO Fe-Si	Fe-Co	Mn-Zn ferrite N87	Nanocrystalline ribbon
Sample	Epstein	Epstein	Ring	Ring
Thickness d (mm)	0.194	0.201	5.09	$20.46 \cdot 10^{-3}$
Density δ (kg/m^3)	7650	8120	4850	7200
Resistivity ρ (Ω m)	$52.0 \cdot 10^{-8}$	$44.0 \cdot 10^{-8}$	9.4	$118.0 \cdot 10^{-8}$
Saturation polarization J_s (T)	2.00	2.35	0.50	1.25

II. EXPERIMENTAL METHOD AND PROCEDURE

Non-oriented Fe-Si and Fe-Co steel sheets, 0.194 mm and 0.201 mm thick, respectively, have been characterized at peak induction $B_p = 1.0$ T up to a few kHz using a 200-turn Epstein magnetizer, according to the IEC 60404-10 Standard. A calibrated hysteresisgraph-wattmeter with digital control of the induction waveform, using an Agilent33220A arbitrary function generator and a DC-10 MHz NF-HSA4101 power amplifier for supplying the primary winding, was employed. Signal detection, conversion, and analysis were made through a 12-bit 500 MHz LeCroy4054A oscilloscope and software (Agilent VEE environment). The digital control of the induction waveform was carried out by means of recursive method, where the desired voltage output $u(t)$ is approached

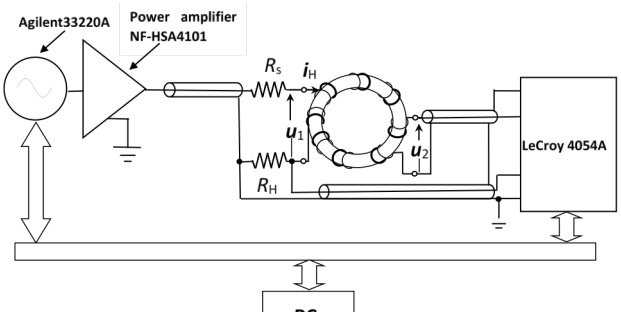

Fig. 1. Hysteresisgraph-wattmeter used to measure the broadband magnetic losses of soft magnetic materials. The induction waveform is controlled regulating the supply current (measured via the voltage drop on the calibrated shunt R_H) by digital feedback. This setup has been used to characterize both the Fe-Si and Fe-Co Epstein strips up to 5 kHz and the Mn-Zn and nanocrystalline ring samples up to 4 MHz. The ring samples are eventually characterized up to 100 MHz by a transmission line method using a Vector Network Analyzer (VNA).

through an iterative procedure, by which the $(n + 1)$th periodic voltage input $e(t)$ is updated by addition of a term linearly dependent on the difference between the desired output and the one obtained at the nth iteration [20]. The scheme of the employed setup is shown in Fig. 1. Besides the conventional characterization under sinusoidal induction, carried out up to f = 5 kHz, energy loss measurements were performed in the non-oriented steel sheets with square wave voltage and duty cycle a ranging between 0.5 and 0.1, as schematically illustrated in Fig. 2. In this case, we start by generating a rectangular voltage with the function generator and we proceed with the recursive procedure till the desired rectangular voltage $V_2(t)$ is obtained on the secondary winding. The same setup was employed to measure nanocrystalline Finemet ribbons of thickness d = 20.46 μm and width w = 10 mm, tapewound as 20 mm diameter rings and annealed under a tranverse saturating field (induced transverse anisotropy $K_\perp \sim 25$ J/m^3) and commercial N87-type Mn-Zn ring samples (outside diameter 15 mm, thickness 5.09 mm). The measurements in these samples were performed up to 1 – 4 MHz at B_p = 100 mT. The primary and secondary windings, their layout, and the connecting cables ensured minimum stray parameters. High-frequency measurements, from a few hundred kHz to 100 MHz, were covered by a transmission line method using an Agilent 8753A Vector Network Analyzer, as discussed in [21]. Such method provides the frequency behavior of the complex permeability $\underline{\mu} = \mu' - j\mu''$ and is obviously restricted to defined exciting power (10 mW in the present case) and sinusoidal signal. But the fluxmetric measurements show that, on approaching the MHz frequencies, μ' and μ'' become independent of B_p, at least below some 100 mT in the Mn-Zn ferrites and 500 mT in the transverse anisotropy nanocrystalline ribbons, and overlap with the VNA measured permeabilities. This occurs at frequencies high enough to induce full relaxation of the domain wall (dw) displacements, much more restrained than the rotations by the dissipative effects. On the other hand, the rotational permeability is relatively independent of B_p, up to about $0.1J_s$ – $0.2J_s$ in ferrites and $0.5J_s$ in the transverse anisotropy nanocrystalline ribbons. It is therefore found that, at sufficiently high frequencies (typically beyond a few hundred kHz), the energy loss fluxmetrically measured at given B_p value tends to coincide with the loss figure calculated from the measured μ' and μ'' through the equation

$$W(B_p, f) = \pi B_p^2 \frac{\mu''}{\mu'^2 + \mu''^2}. \qquad [\text{J/m}^3] \qquad (2)$$

This property is illustrated, together with the behavior of μ', in Fig. 3 for the investigated Mn-Zn ferrite and nanocrystalline samples at B_p = 100 mT. The upper frequency portion of the fluxmetrically obtained results (symbols) are shown to overlap with the lower frequency portion of the VNA determined permeability and loss values. μ' and μ'' suffice then to describe, for defined B_p value, shape and area of the hysteresis loop (quasi-linear response) .

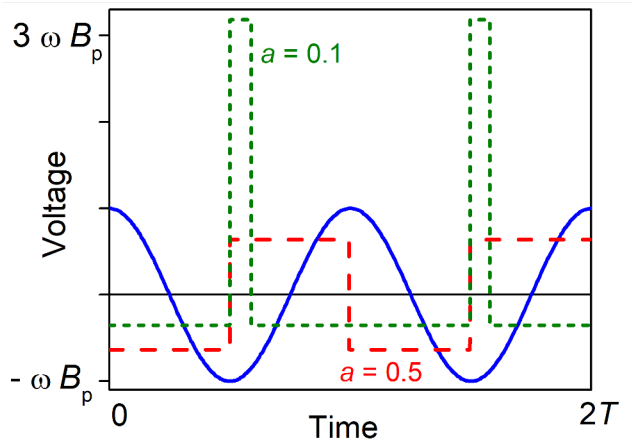

Fig. 2. Example of investigated voltage waveforms for given peak induction B_p: sinusoidal, symmetric square, and asymmetric square with duty cyle a = 0.1.

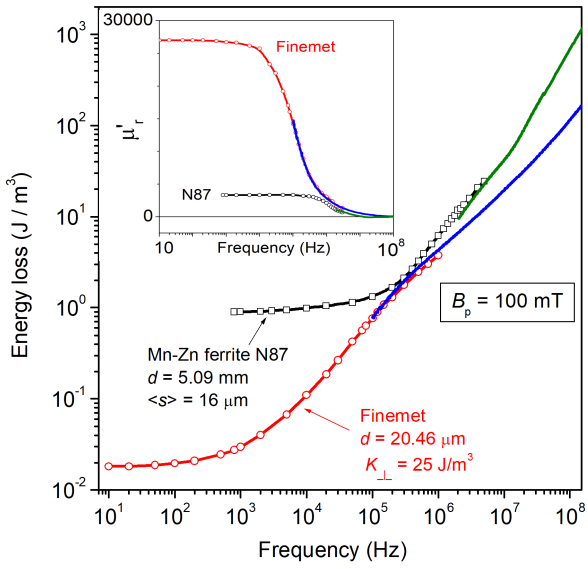

Fig. 3. Broadband behavior of energy losses at B_p = 100 mT in the tapewound transverse anisotropy ($K_\perp$ = 25 J/m^3) Finemet-type nanocrystalline ribbon and in the N87 Mn-Zn ferrite. d ≡ thickness, <s> ≡ average grain size. Symbols: fluxmetric measurements. Solid lines: measurements by transmission line and VNA and use of (2). The inset shows the corresponding frequency dependence of the real relative permeability μ'$_r$.

III. From Sinusoidal to Triangular Symmetric and Asymmetric Induction: Energy Loss Prediction

In this Section we develop first a comprehensive approach to the prediction of magnetic losses under symmetric and asymmetric square-wave voltage in thin ($d \sim 0.20$ mm) non-oriented steel sheets, up to 5 kHz, in Mn-Zn ferrites and in transverse anisotropy ($K_{\perp} \sim 25$ J/m^3) nanocrystalline ribbons up to a few MHz. We verify that skin effect enters into play in the steel sheets around 800 Hz in the Fe-Co sheets and 1500 Hz in the Fe-Si sheets. In order to extend the analysis beyond such frequencies, we describe the magnetic constitutive equation of the material at low and intermediate inductions ($B_p = 1.0$ T in the present measurements) by an equivalent complex permeability. In this way, we can analytically solve the Maxwell's diffusion equation and proceed with the loss decomposition under sinusoidal induction. The Landau-Lifshitz equation is invoked for making explicit the constitutive equation of the Mn-Zn ferrite and nanocrystalline ring samples at high frequencies and for proceeding with loss *decomposition. Examples of experimental and interpretative* results obtained in these materials for $B_p = 100$ mT are given.

A. Losses in non-oriented Fe-Si and Fe-Co sheets

The energy losses under triangular induction waveform at power frequencies can be easily dealt with in magnetic steels sheets starting from standard measurements under sinusoidal induction, resorting to the STL, and formulating in a simple way the energy loss components W_{hyst}, $W_{cl}(f)$, and $W_{exc}(f)$ under generic induction waveform [10], [13]. The condition of negligible skin effect, implying relatively low working frequencies, is, however, required. We provide in Fig. 4 an example concerning the energy losses measured up to $f = 800$ Hz in the 0.201 mm thick $Fe_{49}Co_{49}V_2$ sheet. Following the loss decomposition method, we identify first the waveshape independent hysteresis component $W_{hyst}(B_p) = \lim_{f\to 0} W(B_p, f)$ and calculate the classical loss component

$$W_{cl}(B_p, f) = \frac{\sigma d^2}{12} \cdot \int_0^{1/f} \left(\frac{dB}{dt}\right)^2 dt \qquad [J/m^3] \qquad (3)$$

in the sheet of thickness d and conductivity σ. The appraisal of the dynamics of the Magnetic Objects (mesoscopic regions where the dws move in a tightly correlated fashion [9]), made according to the STL [15], leads to the following general formulation for the excess loss

$$W_{exc}(B_p, f) = \sqrt{\sigma G S V_0(B_p)} \cdot \int_0^{1/f} \left|\frac{dB}{dt}\right|^{3/2} dt, \ [J/m^3] \qquad (4)$$

where $G = 0.1356$, S is the sample cross-sectional area, and $V_0(B_p)$ is a statistical parameter, increasing with B_p. This parameter lumps the role of the microstructure [9]. We can easily specialize (4) to any kind of periodic induction waveform without local minima (i.e. without minor nested hysteresis loops). For sinusoidal $B(t)$ we obtain

$$W_{cl,SIN}(B_p, f) = \frac{\pi^2}{6} \cdot \sigma d^2 B_p^2 f \qquad [J/m^3] \qquad (5)$$

and

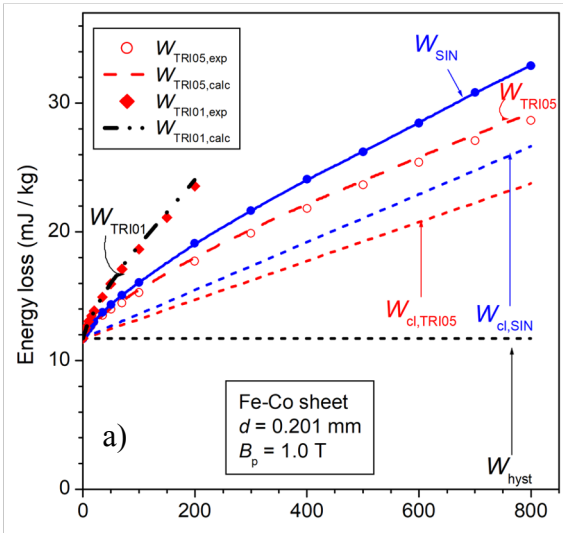

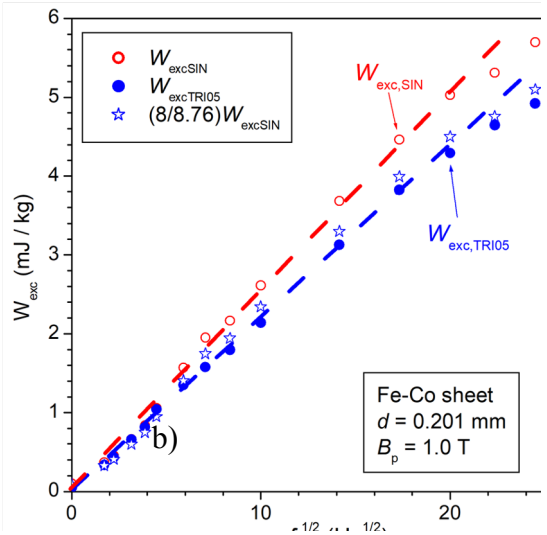

Fig. 4. a) Energy loss in the 0.201 mm thick Fe-Co sheets up to 800 Hz (i.e., up to incipient skin effect) measured under sinusoidal (W_{SIN}) and triangular symmetric (W_{TRI05}) induction (symbols) of peak value $B_p = 1.0$ T. The loss components $W_{cl,TRI05}$ and $W_{exc,TRI05}$ are obtained from the corresponding quantities $W_{cl,SIN}$ and $W_{exc,SIN}$ according to (3) and (4) and $W_{TRI05}(f)$ is consequently calculated by (7) (dashed line). The loss figure W_{TRI01} (symbols) measured with asymmetric triangular $B(t)$ and duty cycle $a = 0.1$, and its prediction (dash-dot line) are also shown up to 200 Hz. b) Excess loss components $W_{exc,SIN}$ and $W_{exc,TRI05}$ versus $f^{1/2}$. They both follow the $f^{1/2}$ law below about 600 Hz. The experimental $W_{exc,TRI05}$ (full symbols) is compared with the predicted quantity $(8/8.76)W_{exc,SIN}$ (open symbols). The dashed lines are a guide to the eye.

$$W_{exc,SIN}(B_p, f) = 8.76\sqrt{\sigma G S V_0(B_p)} \cdot B_p^{3/2} f^{1/2}. \qquad [J/m^3] \quad (6)$$

Using (3) and (4), we conclude that, once the energy loss for sinusoidal induction is known, we can predict the same quantity for triangular symmetric $B(t)$, according to

$$W_{TRI05}(B_p, f) = W_{hyst}(B_p) + W_{cl,TRI05}(B_p, f) + W_{exc,TRI05}(B_p, f) = \\ = W_{hyst}(B_p) + \frac{8}{\pi^2} \cdot W_{cl,SIN}(B_p, f) + k_{exc} \cdot W_{exc,SIN}(B_p, f) \qquad (7)$$

with $W_{hyst}(B_p)$ independent of the $B(t)$ law and the constant k_{exc} = 8/8.76. In some circumstances, as shown in the following, the excess loss is found to follow the power law $W_{exc,SIN}(f) \propto f^p$, with $p > 0.5$ [22]. In this case, the general relationship for W_{exc} applies

$$W_{exc,TRI05}(B_p, f) = k_{exc} \cdot W_{exc,SIN}(B_p, f) \quad , \qquad (8)$$

where $k_{exc} = 4^{(1+p)}/[(2\pi)^p \cdot \int_0^{2\pi} |\cos\alpha|^{(1+p)}\, d\alpha]$ and $\alpha = \omega t$. It is remarked that *a couple of measurements, for given B_p, of $W_{SIN}(B_p, f)$ at two frequencies* suffice in principle to make the loss decomposition and apply (7). The ensuing prediction is shown, as an example, in Fig. 4a (0.201 mm thick Fe-Co sheet, dashed line), compared with the experimental $W_{TRI05}(f)$ at B_p = 1.0 T (open symbols) up to the maximum frequency f = 800 Hz. Fig. 4b shows, in particular, the measured excess losses $W_{exc,SIN}(f)$ and $W_{exc,TRI05}(f)$, both following the $f^{1/2}$ law. The latter is compared with the predicted quantity (8/8.76)·$W_{exc,SIN}(f)$. It is a result easily extrapolated to the case of asymmetric triangular $B(t)$. It suffices to apply (7) twice, for the frequencies f_1 = 1/(2aT) and f_2 = 1/(2(1-a)T), respectively, and average the resulting loss figures. Fig. 4a also shows the measured (symbols) and predicted by (7) (dashed-dotted line) loss $W_{TRI01}(f)$ (symbols), for the asymmetric $B(t)$ with duty cycle a = 0.1.

It is apparent here, besides our capability of transposing in a simple way the theoretical assessment of $W_{SIN}(f)$ into a good prediction of $W_{TRI01}(f)$ by (7), the relatively restricted frequency range of our prediction. This descends from the limitation posed by the appearance of the skin effect above a certain critical frequency f_0 (~ 800 Hz and ~ 1.5 kHz in the Fe-Co and Fe-Si sheets, respectively), with the ensuing deviations of the predictions by (5) and (6) from the actual behaviors of $W_{cl,SIN}(f)$ and $W_{exc,SIN}(f)$. The loss decomposition procedure is indeed affected by the establishment of a non-uniform induction profile across the sheet thickness, a condition whose full treatment requires, because of the non-linear hysteretic constitutive magnetic equation of the material, hysteresis modeling (for example, the Dynamic Preisach Modeling) and numerical methods [23]. It is a cumbersome procedure, of little practical appeal, and it might be appropriate to look for a much simpler approach, if worth the price to pay in terms of predicting accuracy. The conventional approach to the eddy current losses in a magnetic sheet of thickness d (-d/2 ≤ z ≤ d/2) with AC field applied along the y-direction consists in solving, with appropriate boundary conditions, the Maxwell's diffusion equation

$$\frac{\partial^2 H_y(z)}{\partial z^2} = \sigma\mu \frac{\partial H_y(z)}{\partial t} \qquad (9)$$

in a hypothetical structureless material with linear DC constitutive equation $B = \mu H$. The classical loss is obtained as

$$W_{cl,SIN}(B_p, f) = \frac{\pi}{2} \cdot \frac{\lambda B_p^2}{\mu} \cdot \frac{\sinh\lambda - \sin\lambda}{\cosh\lambda - \cos\lambda}, \quad [J/m^3] \qquad (10)$$

where $\lambda = \sqrt{\pi\sigma\mu d^2 f}$ [9]. The gross approximation involved with a linear constitutive equation leads, however, to poor prediction of $W_{SIN}(B_p, f)$ at high frequencies. Aiming thus at a realistic analytical formulation approximately accounting for hysteresis, we emulate the constitutive magnetic equation, as given by the quasi-static hysteresis loop of peak induction B_p, by an equivalent complex permeability, that is, an elliptical loop of identical area $W_{hyst}(B_p) = \pi B_p^2 (\mu''/(\mu'^2 + \mu''^2))$ and same B_p value. With $B_p = \sqrt{\mu'^2 + \mu''^2}\, H_p$, we can also write $W_{hyst}(H_p) = \pi H_p^2 \mu''$. With these two independent conditions, we obtain the real and imaginary permeability components as μ' = 0.0159 $TA^{-1}m^{-1}$ and μ'' = 0.0121 $TA^{-1}m^{-1}$ in the Fe-Co sheets, μ'=0.0100 $TA^{-1}m^{-1}$ and μ'' = 0.0078 $TA^{-1}m^{-1}$ in the Fe-Si ones. Under quasi-static conditions, we assign these relationships both local and macroscopic character. The local static relationships are defined, over the here investigated frequency range, once and for all. The macroscopic ones, involving the applied field and the induction averaged over the sample cross-section, evolve with frequency. We are interested in predicting such an evolution. The involved approximations are obviously expected to apply better at low inductions and to comply with the frequency response of the material up to relatively mild non-uniform induction profiles. By introducing the previously defined complex $\underline{\mu}$ in the diffusion equation (9), now written as

$$\frac{\partial^2 \underline{H}_y(z)}{\partial z^2} = j\omega\sigma\underline{\mu}\,\underline{H}_y(z) \quad , \qquad (11)$$

with the appropriate boundary conditions, we eventually arrive at the following analytical formulations for the frequency dependence of hysteresis and classical losses in the presence of skin effect

$$W_{hyst}(B_p, f) = = \frac{\pi B_P^2}{2|\underline{\mu}|} \frac{\mu''}{\mu'} \frac{(\lambda' + \lambda'')\sinh(\lambda' - \lambda'') + (\lambda' - \lambda'')\sin(\lambda' + \lambda'')}{\cosh(\lambda' - \lambda'') - \cos(\lambda' + \lambda'')}. \qquad (12)$$

$$W_{cl,SIN}(B_p, f) = = \frac{\pi}{2} \frac{B_P^2}{\mu'} \cdot \frac{(\lambda' + \lambda'')\sinh(\lambda' - \lambda'') - (\lambda' - \lambda'')\sin(\lambda' + \lambda'')}{\cosh(\lambda' - \lambda'') - \cos(\lambda' + \lambda'')}, \qquad (13)$$

where the complex quantity λ = λ' + jλ'' is related to the complex permeability through to the equation

$$\lambda = \sqrt{\frac{\omega\sigma|\underline{\mu}|d^2}{2}} \cdot \left(\sqrt{\frac{1 + \mu'/|\underline{\mu}|}{2}} - j \cdot \sqrt{\frac{1 - \mu'/|\underline{\mu}|}{2}} \right). \qquad (14)$$

Equations (12) and (13) reduce to $W_{hyst}(B_p) = \lim_{f\to 0} W(B_p, f)$ and (5), respectively, for f < ~ 5/(πσ|μ|d^2). The full procedure by which the diffusion equation (11) leads to (12) and (13) is discussed in the Appendix. We have no equivalent formulation for the excess loss component $W_{exc}(B_p, f)$, which can only be obtained by making the difference between the experimental loss $W(f)$ and the sum $W_{hyst}(B_p, f) + W_{cl,SIN}(B_p, f)$. An example of the so obtained loss decomposition is shown, for the Fe-Co and Fe-Si sheets measured at B_p = 1.0 T up to 5 kHz, in Figs. 5 and 6, respectively. Under increasing frequencies, the sample

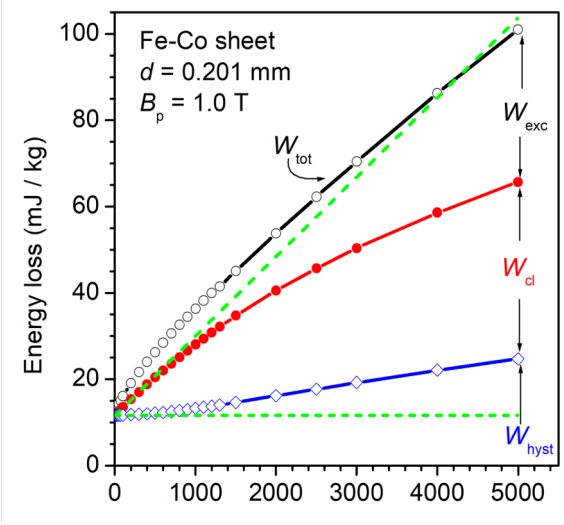

Fig. 5. Broadband loss analysis in the 0.201 mm thick Fe-Co sheets of Fig. 4, carried out under sinusoidal induction of peak value B_p = 1.0 T up to 5 kHz. $W_{hyst}(f)$ and $W_{cl,SIN}(f)$ are calculated using (12) and (13), based on the assumption of a constitutive $B(H)$ equation defined in terms of complex permeability. To note the increase of W_{hyst} and the non-linear behavior of $W_{cl,SIN}$ versus frequency. The dashed lines show the frequency dependence of $W_{hyst}(f)$ and $W_{cl,SIN}(f)$ predicted disregarding the skin effect. This actually starts to affect the magnetization process beyond about 800 Hz.

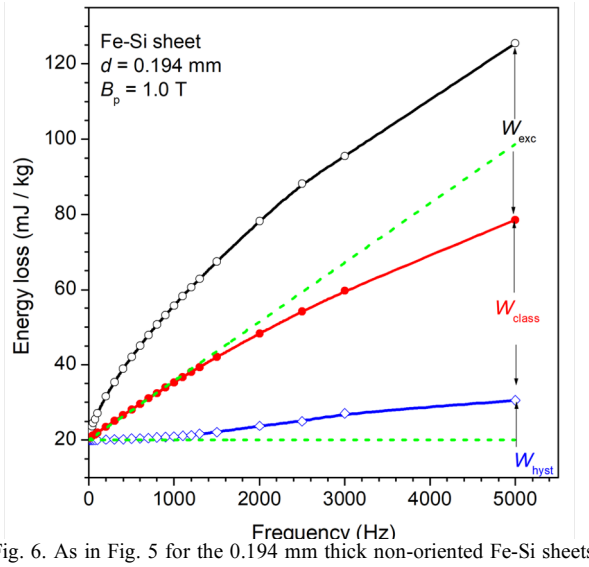

Fig. 6. As in Fig. 5 for the 0.194 mm thick non-oriented Fe-Si sheets. The components $W_{hyst}(f)$ and $W_{cl,SIN}(f)$ are calculated using (12) and (13). The effect of the frequency dependent non-uniform induction profile becomes apparent beyond about 1500 Hz, where the conventional prediction disregarding the skin effect (dashed lines) departs from the abovementioned calculation.

falls into a condition of non-uniform induction profile. By the previous equations we obtain, in particular, that W_{hyst} starts to increase and $W_{cl,SIN}(f)$ attains a less than linear increase with f beyond about 800 Hz in Fe-Co and 1500 Hz in Fe-Si. This contrasts with the behaviors predicted for these quantities by the conventional equation (5) (dashed lines).

We connect now the so-defined broadband loss components $W_{hyst}(f)$, $W_{cl,SIN}(f)$, and $W_{exc,SIN}(f)$ with the same quantities associated with the symmetric and asymmetric triangular induction. We calculate $W_{TRI05}(f)$ with (7), by posing $W_{cl,TRI05}(f) = (8/\pi^2)\cdot W_{cl,SIN}(f)$ and $W_{exc,TRI05}(f) = (8/8.76)\cdot W_{exc,SIN}(f)$ over the full frequency range. The total loss for triangular $B(t)$ is thus predicted, as previously discussed, as shown in Fig. 7 and Fig. 8 for the Fe-Co and Fe-Si sheets, respectively. Here, in particular, the experimental broadband energy losses $W_{TRI}(f)$ associated with the duty cycles a = 0.5, 0.2, and 0.1 (symbols) are shown to compare well with the prediction made by (7), starting from the calculated sinusoidal components $W_{hyst}(f)$, $W_{cl,SIN}(f)$, and $W_{exc,SIN}(f)$.

B. Nanocrystalline ribbon and Mn-Zn ferrite. Broadband analysis.

The good soft magnetic properties of the transverse anisotropy nanocrystalline ribbons and the Mn-Zn ferrites extend deeply in the MHz region, as shown in Fig. 3. Here, in particular, one can appreciate the excellent frequency response of the nanocrystalline samples, which combine high Snoek's product with low losses at all frequencies. The low value of the anisotropy constant and the ensuing prominent role of magnetization rotations are indeed instrumental in promoting such behavior of Mn-Zn ferrites and nanocrystalline alloys. However, the quantitative assessment of the loss properties over the many-decade frequency range useful for applications reveals a complex task. To simplify the matter, quasi-linear DC constitutive equation is therefore assumed, so that the concept of complex permeability and related energy loss, according to (2), applies [24], [25], [26]. The shape of the actually measured DC hysteresis loops (B_p = 0.1 T), shown Fig. 10, ensures that the description of their frequency evolution in terms of complex permeability provides a good approximation.

Fast stroboscopic Kerr observations performed on the transverse anisotropy nanocrystalline ribbons show a relatively sharp transverse domain structure and both rotational and dw processes in response to an applied longitudinal AC field [27]. The activity by the transverse dws is caused by magnetostatic conditions at the ribbon edges evolving with the field amplitude. The dw displacements, which do not contribute to net sample magnetization, are observed to progressively relax under increasing frequency, eventually coming to a halt on approaching the MHz range. Here, only the rotations survive. Consequently, the loss phenomenology attains a classical character, the one pertaining to a quasi-homogeneous rotational process. We note, however, that the slope of the $W(f)$ curve in the MHz range (Fig. 3) is higher than the $f^{1/2}$ law predicted by the Maxwell's equations for the investigated metallic ribbons [9]. Such a power law would be in fact expected to hold beyond about 1 MHz, where the skin effect is predicted to appear, according to (9) and the value of the DC permeability $\mu_{r,DC} = 27\cdot10^3$. Actually, we know that the magnetic constitutive equation pertaining to the rotations evolves at high frequencies in obedience to the Landau-Lifshitz (LL) equation [28]. By introducing then the solution of the LL equation, expressed in terms of complex permeability, in the Maxwell's diffusion equation (11), we can eventually derive an analytical expression for the rotational classical loss $W_{rot}(B_p, f)$. This approach is fully discussed in [25]. It leads to the loss decomposition procedure for sinusoidal induction, shown up to 100 MHz in Fig. 10, where we separate $W_{rot}(f)$ from the d.w.

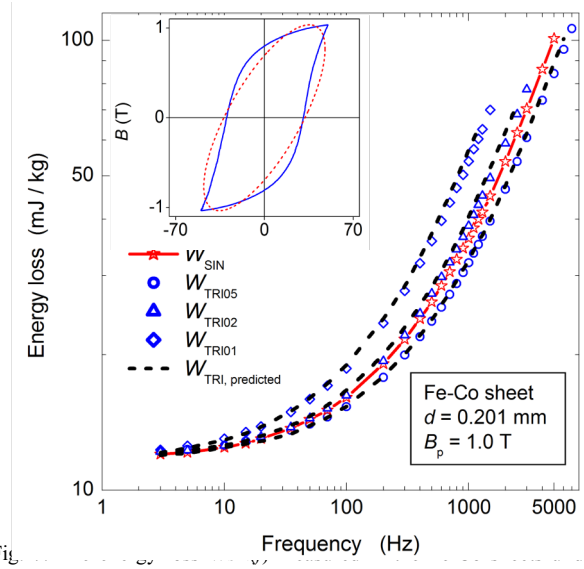

Fig. 8. As in Fig. 7 for the Fe-Si sheets.

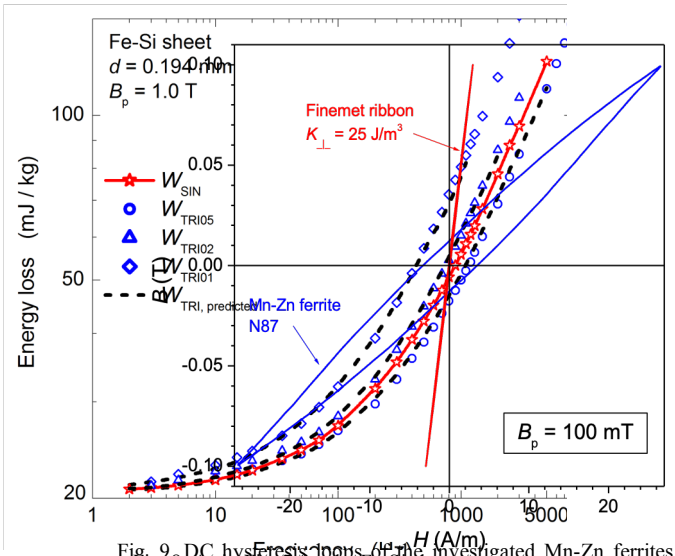

Fig. 9. DC hysteresis loops of the investigated Mn-Zn ferrites and transverse anisotropy nanocrystalline Finemet ribbons at B_p = 0.1 T. We describe their evolution with frequency in terms of complex permeability, so that the energy loss $W(B_p, f)$ can, in particular, be expressed by (2).

sinusoidal $B((t)$ for B_p = 1.0 T is compared, up to 5 kHz, with the same quantity, measured at the same B_p value under symmetric triangular ($W_{TRI05}(f)$), and asymmetric triangular $B((t)$, with duty cycles $0.2T$ ($W_{TRI02}(f)$ and $0.1T$ ($W_{TRI01}(f)$ (symbols). The dashed fitting lines ($W_{TRI,predicted}$) are obtained starting from the decomposition of $W_{SIN}(f)$, made according to (12) and (13), and applying (7) twice, for the frequencies $f_1 = 1/(2aT)$ and $f_2 = 1/(2(1-a)T)$, respectively. The inset compares the experimental quasi-static hysteresis loop at B_p = 1.0 T with the equivalent elliptical loop (same B_p value and area), analytically defined through the real μ' and imaginary μ'' permeability components.

contribution $W_{dw}(f)$ by subtracting it from the measured loss $W_{dw}(f) = W(f) - W_{rot}(f)$. We note in Fig. 10 the drop of $W_{dw}(f)$ beyond a few hundred kHz, following the relaxation of the dw processes. We can further subdivide $W_{dw}(f)$ into the static and dynamic loss components $W_{dw}(f) = W_{hyst} + W_{exc}(f)$. The latter is shown in the inset of Fig. 10. It exhibits a power law dependence on frequency $W_{exc}(f) \propto f^{0.75}$, against the typical $W_{exc}(f) \propto f^{0.50}$ displayed by the steel sheets in the absence of skin effect (see Fig. 4b).

There are good phenomenological similarities between the magnetic loss behavior of the transverse anisotropy nanocrystalline ribbons and the sintered Mn-Zn ferrites, because of a similarly important role of the moment rotations. In ferrites, rotations are favored by the intrinsically low value of the magnetocrystalline anisotropy, ensuing from the phenomenon of anisotropy compensation [29]. But the major dissipation mechanism in ferrites is related to the spin damping and the eddy currents play a role only at very high frequencies in sufficiently large samples [24]. Again, the LL equation is invoked for dealing with the rotational processes. Real and imaginary rotational permeabilities are calculated as solutions of the LL equation by assuming distributed effective anisotropy fields, that is, ferromagnetic resonance frequencies changing from grain to grain. The rotational (classical) loss $W_{rot}(B_p, f)$ is then obtained with (2), after suitable integration over the distribution functions for amplitude and orientation of the anisotropy fields. A detailed discussion on the physical assumptions and the performed calculations, including the possible contribution by eddy currents in sufficiently thick specimens, is given in [24] [26]. Fig. 10 shows the so-obtained loss decomposition in the N87 Mn-Zn ring samples. $W_{dw}(f)$ drops beyond a few MHz, denoting full relaxation of the dw processes. It is also noted that $W_{exc}(f) \propto f^{0.82}$.

With the so-calculated loss components W_{hyst}, $W_{rot,SIN}(f)$ (i.e. $W_{cl,SIN}(f)$), and $W_{exc,SIN}(f)$, we apply again (7), in order to predict $W(f)$ in the nanocrystalline and ferrite samples under triangular symmetric and asymmetric $B(t)$. W_{hyst} is independent of frequency and $B(t)$ waveshape. Non-uniform induction profile due to the skin effect can in fact be safely excluded, at least in the frequency range where the contribution by W_{hyst} is not negligible [24][25]. Eddy current losses are actually shown to play a role in the 5 mm thick N87 ferrite samples only beyond a few MHz [24]. At the same time, the skin effect in the nanocrystalline ribbon is restrained by the exchange field [30]. In order to derive $W_{TRI}(f)$ from the decomposed $W_{SIN}(f)$ we start by posing $W_{rot,TRI}(f) = (8/\pi^2) \cdot W_{rot,SIN}(f)$, a simplifying and

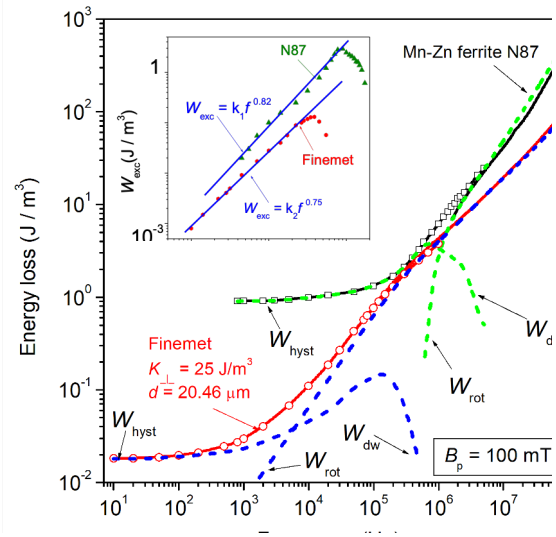

Fig. 10. Loss decomposition up to 100MHz in the N87 Mn-Zn ferrite and in the transverse anisotropy ($K_\perp = 25$ J/m^3) nanocrystalline Finemet ribbon (sinusoidal $B(t)$). The experimental $W(f)$ is shown by symbols (fluxmetric) and solid lines (VNA). The rotational loss component W_{rot}, which plays the role of classical loss W_{cl}, is theoretically predicted and separated from the domain wall contribution $W_{dw} = W_{hyst} + W_{exc}$. W_{dw} is bound to decrease and eventually disappear at high frequencies, following the relaxation of the domain wall displacements. The excess loss $W_{exc} = W_{dw} - W_{hyst.}$, shown in the inset, displays a power law dependence on frequency $W_{exc} \propto f^n$, with $n > 0.5$.

relatively crude approximation for the Mn-Zn ferrite, where the slope of the predicted $W_{rot,SIN}(f)$ undergoes a rapid change around 1-2MHz. We take then k_{exc} according to (8) and the obtained power law $W_{exc,SIN}(f) \propto f^p$ (inset in Fig. 10), to find $k_{exc} = 0.86$ and $k_{exc} = 0.84$ for the nanocrystalline and Mn-Zn samples, respectively. The losses for triangular symmetric and asymmetric induction are finally calculated through (7) and

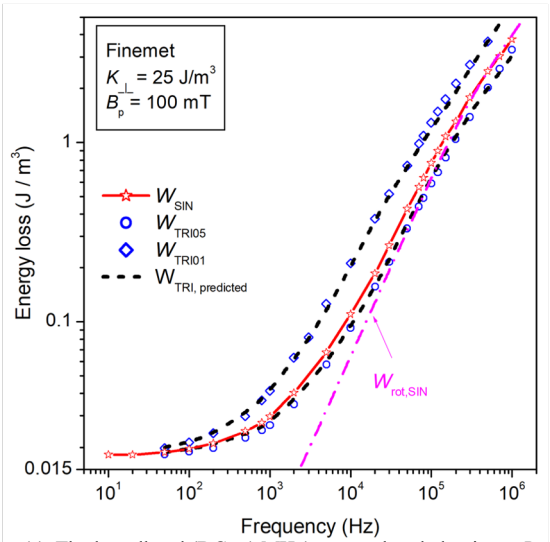

Fig. 11. The broadband (DC - 1 MHz) energy loss behavior at $B_p = 100$ mT under triangular symmetric (W_{TRI05}) and asymmetric (W_{TRI01}, duty cycle $a = 0.1$) induction, measured in the nanocrystalline Finemet transverse anisotropy tapewound ring sample (symbols), is compared with the same quantity $W_{SIN}(f)$ (line and symbols) measured with sinusoidal induction. By making the loss decomposition of $W_{SIN}(f)$, illustrated in Fig. 10, and applying (7), $W_{TRI05}(f)$ and $W_{TRI01}(f)$ are predicted (dashed lines).

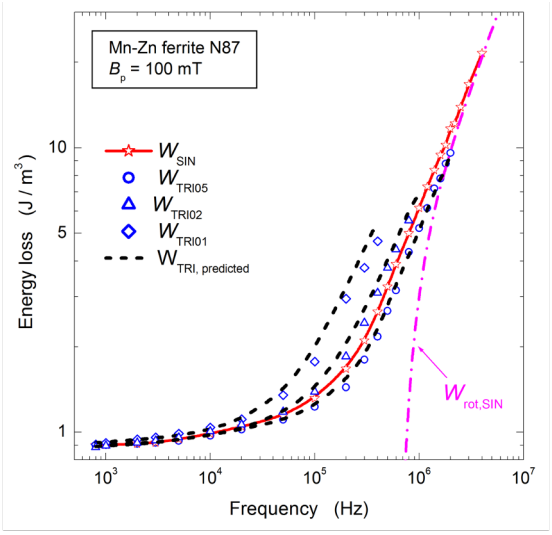

Fig. 12. Same as Fig. 11 for the Mn-Zn ferrite. Besides the loss under triangular symmetric induction $W_{TRI05}(f)$, the same quantity for asymmetric induction, with duty cycles $a = 0.2$ ($W_{TRI02}(f)$) and $a = 0.1$ ($W_{TRI01}(f)$) is measured (symbols) and predicted (dashed lines), starting from the loss components of $W_{SIN}(f)$ and applying (7).

compared with the experimental $W_{TRI05}(f)$, $W_{TRI02}(f)$, and $W_{TRI01}(f)$ behaviors, as shown in Fig. 11 and Fig. 12 for the nanocrystalline and the Mn-Zn samples, respectively.

It might be argued that the here proposed method would not fully cover the case where a DC field bias is applied to the magnetic core. However, this problem can be mitigated to some extent. Regarding the Fe-Si sheets, we can estimate, based on the study reported in [19], which shows that the bias mainly affects W_{hyst}, that at intermediate frequencies (say around 2 kHz) and $J_{bias} = 0.75$ T, we can expect an increase of the loss of the order of 5 % for $J_p = \pm 1.0$ T. In the Fe-Co the increase should be lower, of the order of 2 %, for a same J_p swing and $J_{bias} = 1.5$ T. Negligible variation is expected in the nanocrystalline ribbons, because of their extended $J(H)$ linearity, while a substantial effect might be appreciated in the Mn-Zn ferrites. It is nevertheless important to stress that the classical loss component $W_{cl}(J_p, f)$, (be it due to eddy currents or spin damping) is quite independent of the field bias. Consequently, it suffices to measure $W(f)$ under DC bias and sinusoidal induction and calculate $W_{rot,SIN}(J_p, f)$, as previously discussed, to achieve loss separation. It is then an easy matter to pass, according to (7), to the symmetric/asymmetric square voltage regime. Such a regime, with its extended harmonics spectrum, would prove quite challenging for direct measurements. Good practical advantage is thus achieved by relying on the much more affordable sinusoidal induction measurement.

IV. Conclusions

Symmetric and asymmetric squared voltage waveforms are frequently imposed on inductive components for power electronics. The usual approach to the prediction of the magnetic losses under such working conditions is based on a suitable generalization of the Steinmetz's equation. The fully empirical character of such equation calls, however, for the introduction of a range of fitting parameters, depending on peak

induction level, frequency, and duty cycle. Besides bearing undistinguished scientific value, this method results into somewhat restricted domain of application under a reasonably restricted range of parameters. In this work, we demonstrate that, starting from the physical background provided by the Statistical Theory of Losses and the associated concept of loss decomposition, we can provide a good predicting approach to the frequency dependence of the magnetic losses under symmetric and asymmetric triangular induction, upon a remarkably broad range of frequencies and with different types of soft magnetic materials. We show, in particular, that this is achieved using only basic knowledge of the material response under sinusoidal flux (i.e. voltage), by which the loss components (hysteresis, classical, and excess) are derived. Such a response is, in turn, predictable with minimum information on the Fe-Si and Fe-Co sheets (conventional measurement of the quasi-static hysteresis loop and the energy loss at 50 Hz), while broadband fitting for sinusoidal flux is desirable in the Mn-Zn samples and the nanocrystalline alloy. The fundamental step, in any case, is the derivation of the classical loss, for which analytical formulation is provided.

Fe-Si and Fe-Co non-oriented sheets have been characterized up to about 5 kHz at peak induction $B_p = 1.0$ T. By entering the kHz range, skin effect takes place in these sheets. Consequently, modeling is performed exploiting the additional knowledge of the DC hysteresis loop and the best fitting of it using the complex permeability. This plays the role of constitutive magnetic equation, to be used in the calculation of the classical loss $W_{cl,SIN}(f)$ by the Maxwell's diffusion equation.

Transverse anisotropy nanocrystalline ribbons and Mn-Zn ferrite samples have been measured at $B_p = 100$ mT up to about 1 MHz. Again, loss decomposition for sinusoidal $B(t)$ is performed, but the calculation of $W_{cl,SIN}(f)$ upon the involved high-frequency range calls for the calculation of the dynamic constitutive equation of the material. This concerns, in particular, the rotational processes, largely prevailing on the domain wall displacements. We thus obtain the complex permeability versus frequency as a solution of the Landau-Lifshitz equation. This provides a frequency dependent magnetic constitutive equation. With the loss components for sinusoidal voltage at our disposal, the response of the material to imposed symmetric and asymmetric square-wave voltage can thus be predicted, making use of a couple of known constants. The role of the DC field bias, though not explicitly accounted for, is predictably decreasing with increasing frequencies and can be approximately estimated relying on the determination of the bias-independent classical loss under sinusoidal voltage and the ensuing loss separation.

REFERENCES

[1] G. Di Capua and N. Femia, "A novel method to predict the real operation of ferrite Inductors with moderate saturation in switching power supply," *IEEE Trans. Power. Electron.*, vol. 31, no. 3, pp. 2456-2564, March. 2016. doi: 10.1109/TPEL.2015.2438952.

[2] J. Reinert, A. Brockmeyer, and R.W.A.A De Doncker, "Calculation of losses in ferro-and ferromagnetic materials based on the modified Steinmetz equation," *IEEE Trans. Ind. Appl.*, vol. 37, pp. 1055–1061, Aug. 2001. doi: 10.1109/28.936396.

[3] J. Li, T. Abdallah, and C Sullivan, "Improved calculation of core loss with nonsinusoidal waveforms," *Proc. IEEE Ind. Appl. Soc. Ann. Meet.*, Oct. 2001, pp. 2203-2210. doi: 10.1109/IAS.2001.955931.

[4] K. Venkatachalam, C.R. Sullivan, T. Abdallah, and H. Tacca, "Accurate prediction of ferrite core losses with nonsinusoidal waveforms using only Steinmetz parameters," *Proc. 8th IEEE Workshop Comput. Power Electron.*, 2002, pp. 36-41.

[5] J. Mülethaler, J. Biela, J.W. Kolar, ans A. Ecklebe, "Improved core loss calculation for magnetic components employed in power electronic systems," *IEEE Trans. Power. Electron.*, vol. 27, no. 2, pp. 964–973, Febr. 2012. doi: 10.1109/TPEL.2011.2162252.

[6] A. P. Van den Bossche, D. M. Van de Sype, and V. C. Valchev, "Ferrite loss measurement and models in half bridge and full bridge waveforms," *Proc. IEEE PESC*, 2005, pp. 1535–1539. DOI: 10.1109/PESC.2005.1581834.

[7] W. Shen, F. Wang, D. Boroyevic, and W. Tipton,IV, "Loss characterization and calculation of nanocrystalline cores for high-frequency applications," *IEEE Trans. Power. Electron.*, vol. 23, no. 1, pp. 475–484, Jan. 2008. doi: 10.1109/TPEL.2007.9111881.

[8] S. Barg, K. Ammous, H. Mejibri, and A. Ammous, "An improved empirical formulation for magnetic core losses estimation under nonsinusoidal induction," *IEEE Trans. Power. Electron.*, vol. 32, no. 3, pp. 2146-2154, March 2017. doi: 10.1109/TPEL.2016.2555359.

[9] G. Bertotti, *Hysteresis in Magnetism*, San Diego, CA, USA, 1998, pp. 391-430.

[10] F. Fiorillo and A. Novikov, "An improved approach to power losses in magnetic laminations under nonsinusoidal induction waveform," *IEEE Trans.Magn.*, vol. 26, no. 5, pp. 2904-2910, Sept. 1990. doi: 10.1109/20.104905.

[11] F. Fiorillo, C. Appino and M. Barisoni, "Power losses in magnetic laminations with trapezoidal induction waveform," *Anales de Fisica, Serie B*, vol. 86, pp. 238-240, 1990.

[12] K. Atallah, Z.Q. Zhu, and D. Howe, "An improved method for predicting iron losses in brushless permanent magnet DC drives," *IEEE Trans.Magn.*, vol. 28, no. 5, pp. 2997-2999, Sep. 1992. doi: 10.1109/20.179696.

[13] M. Amar and F. Protat, "A simple method for estimation of power losses in silicon iron sheets under alternating pulse voltage excitation," *IEEE Trans.Magn.*, vol. 30, no. 2, pp. 942-944, March 1994. doi: 10.1109/20.312453.

[14] R. Kaczmarek, M. Amar and F. Protat, "Iron loss under PWM voltage supply on Epstein frame and in induction motor core," *IEEE Trans.Magn.*, vol. 32, no. 1, pp. 189-194, Jan. 1996. doi: 10.1109/20.477571.

[15] E. Barbisio, F. Fiorillo, and C. Ragusa, "Predicting loss in magnetic steels under arbitrary induction waveform and with minor hysteresis loops," *IEEE Trans. Magn.*, vol. 40, no. 4, pp. 1810-1819, July 2004. doi: 10.1109/TMAG.2004.830510.

[16] W. Roshen, "A practical, accurate and very general core loss model for nonsinusoidal waveforms," *IEEE Trans. Power Electron.* vol. 22, no. 1, pp. 30-40, Jan. 2007. doi: 10.1109/TPEL.2006.8886608.

[17] A. Hilal, M.A. Raulet, C. Martin, and F. Sixdenier, " Power loss prediction and precise modeling of magnetic powder components in DC-DC power converter application," *IEEE Trans. Power Electron.* vol. 30, no. 4, pp. 2232-2237, Apr. 2015. doi: 10.1109/TPEL.2014.2330952.

[18] A.P. Van den Bossche, V.C. Valchev, D. Van de Sype, and L.P. Vandenbossche, "Ferrite losses with square wave voltage and dc bias," J. Appl. Phys., vol. 99, 08M908, 2006. doi: 10.1063/1.2173955.

[19] O. de la Barrière, C. Ragusa, C. Appino, and F. Fiorillo, "Prediction of energy losses in soft magnetic materials under arbitrary Induction waveforms and DC bias," *IEEE Trans. Ind. Electron.*, vol. 64, no. 3, pp. 2522-2529, March 2017. doi: 10.1109/TIE.2016.2608886.

[20] C. Ragusa and F. Fiorillo, "A three-phase single sheet tester with digital control of flux loci based on the contraction mapping principle", *J. Magn. Magn. Mater.*, vol. 304, pp. e568-e570, 2006. doi:10.1016/j.jmmm.2006.02.177.

[21] F. Fiorillo, "Measurements of magnetic materials," *Metrologia*, vol 47, pp. S114-S142, 2010. doi:10.1088/0026-1394/47/2/S11

[22] G. Bertotti, "General properties of power losses in soft ferromagnetic materials," *IEEE Trans. Magn.*, vol. 24, no. 1, pp. 621-630, Jan. 1988. doi: 10.1109/20.43994.

[23] V. Basso, G. Bertotti, O. Bottauscio, F. Fiorillo, M. Pasquale, M. Chiampi, and M. Repetto, "Power losses in magnetic laminations with hysteresis: finite element modeling and experimental validation," *J. Appl. Phys.* vol. 81, no. 8, pp. 5606-5608, April 1997. doi: 10.1063/1.364614.

[24] F. Fiorillo, C. Beatrice, O. Bottauscio, and E. Carmi, "Eddy current losses in Mn-Zn ferrites," *IEEE Trans. Magn.*, vol. 50, no. 1, pp. 6300109, Jan. 2014. doi: 10.1109/TMAG.2013.2279878.

[25] C. Beatrice, S. Dobák, E. Ferrara, F. Fiorillo, C. Ragusa, J, Füzer, and P. Kollár, "Broadband magnetic losses of nanocrystalline ribbons and powder cores," *J. Magn. Magn. Mater.*, vol. 420, pp. 317-323, 2016. doi: 10.1016/j.jmmm.2016.07.045.

[26] C. Beatrice, V. Tsakaloudi, S. Dobák, V. Zaspalis, and F. Fiorillo, "Magnetic losses versus sintering treatment in Mn-Zn ferrites," *J. Magn. Magn. Mater.*, vol. 429, pp. 129-137, 2017. doi: 10.1016/j.jmmm.2016.12.121.

[27] A. Magni, C. Beatrice, O. Bottauuscio, A. Caprile, E. Ferrara, and F. Fiorillo, "Magnetization process in thin laminations up to 1 GHz," *IEEE Trans. Magn.*, vol. 48, no. 4, pp. 1363-1366, April 2012. doi: 10.1109/TMAG.2011.2172934.

[28] K. Seemann, H. Leiste, and V. Bekker, "New theoretical approach to the RF-dynamics of soft magnetic FeTaN films for CMOS components," *J. Magn. Magn. Mater.*, vol. 278, pp. 200-207, 2004. doi: 10.1016/j.jmmm.2003.11.402.

[29] H. Pascard, "Basic concepts for high permeability in soft ferrites," *J. Phys.* (*France*), vol. 8, pp. 377-384, 1998.

[30] O. Bottauscio, F. Fiorillo, C. Beatrice, A. Caprile, and A. Magni, "Modeling high-frequency magnetic losses in transverse anisotropy amorphous ribbons," *IEEE Trans. Magn.*, vol. 51, no. 3, pp. 2800304, March 2015. doi: 10.1109/TMAG.2014.2361534.

APPENDIX

As highlighted in Section III.A, we introduce the complex permeability $\underline{\mu}$, approximating the true magnetic constitutive equation of the material, in the diffusion equation (9). We write

$$\frac{\partial^2 \underline{H}_\mathrm{y}(z)}{\partial z^2} = j\omega\sigma\underline{\mu}\,\underline{H}_\mathrm{y}(z) \qquad \text{(A1)}$$

and we apply the appropriate boundary conditions. The condition $(\mathrm{d}\underline{H}_\mathrm{y}(z)/\mathrm{d}z)_{z=0} = 0$ is dictated by the symmetry of the problem. A further boundary condition is obtained by integrating (A1) over $0 \le z \le d/2$

$$(\mathrm{d}\underline{H}_\mathrm{y}(z)/\mathrm{d}z)_{z=d/2} = j\omega\sigma\int_0^{d/2}\underline{B}_y(z)\,\mathrm{d}z = \frac{d}{2}\cdot j\omega\sigma B_\mathrm{p}, \qquad \text{(A2)}$$

where B_p is the average of the peak induction across the sheet thickness. We obtain the solution

$$\underline{H}_\mathrm{y}(z) = j\omega\sigma B_\mathrm{p}\cdot\frac{d}{2}\cdot\frac{\cosh(kz)}{k\cdot\sinh(kd/2)}, \qquad \text{(A3)}$$

where k is the complex quantity

$$k = \frac{1+j}{\sqrt{2}}\cdot\sqrt{\omega\sigma\underline{\mu}}\,. \qquad \text{(A4)}$$

The field value at the sheet surface $\underline{H}_\mathrm{y}(d/2)$, coincident with the applied field $\underline{H}_\mathrm{ay}$, is therefore related to the peak macroscopic induction according to

$$\underline{H}_\mathrm{y}(d/2) = j\omega\sigma B_\mathrm{p}\cdot\frac{d}{2k}\cdot\coth(kd/2). \qquad \text{(A5)}$$

We pose

$$k = \frac{1+j}{\sqrt{2}}\cdot\sqrt{\omega\sigma\underline{\mu}} = (1+j)\frac{\lambda}{d} \qquad \text{(A6)}$$

and after some algebra we write the complex quantity λ as

$$\lambda = \lambda' + j\lambda'' = \sqrt{\frac{\omega\sigma|\underline{\mu}|d^2}{2}}\cdot\left(\sqrt{\frac{1+\mu'/|\underline{\mu}|}{2}} - j\cdot\sqrt{\frac{1-\mu'/|\underline{\mu}|}{2}}\right) \qquad \text{(A7)}$$

and the complex power

$$S(f) = \frac{1}{2}j\omega B_\mathrm{p}\cdot\underline{H}_\mathrm{y}^*(d/2) = \frac{\pi^2}{6}\sigma d^2 B_\mathrm{p}^2 f^2\cdot\frac{3\coth(k^*d/2)}{k^*d/2}. \qquad \text{(A8)}$$

By taking the real part of $S(f)$, we obtain the energy loss, interpreted as the sum of the hysteresis and classical components, both depending on frequency

$$W_\mathrm{hyst}(f) + W_\mathrm{cl,SIN}(f) = \Re e\,(S(f))/f = \frac{\pi}{2}\cdot\frac{B_\mathrm{p}^2}{|\underline{\mu}|}\cdot\frac{(\lambda'-\lambda'')\sinh(\lambda'-\lambda'') - (\lambda'+\lambda'')\sin(\lambda'+\lambda'')}{\cosh(\lambda'-\lambda'') - \cos(\lambda'+\lambda'')}\ \text{[J/m}^3\text{]} \qquad \text{(A9)}$$

$W_\mathrm{hyst}(f)$ can be singled out in (A9) by integrating the product of local field and induction derivative

$$W_\mathrm{hyst}(B_\mathrm{p},f) = \frac{2}{d}\int_0^{d/2}\mathrm{d}z\int_0^{1/f}H_\mathrm{y}(z,t)\cdot\frac{\mathrm{d}B_\mathrm{y}(z,t)}{\mathrm{d}t}\mathrm{d}t = \pi\frac{2}{d}\int_0^{d/2}\Re\mathrm{e}\left(\underline{H}_\mathrm{y}(z)\cdot j\underline{\mathrm{B}}_\mathrm{y}(z)\right)\mathrm{d}z, \qquad \text{(A10)}$$

which is eventually written as

$$W_\mathrm{hyst}(B_\mathrm{p},f) = \pi\frac{\mu''}{|\underline{\mu}|^2}\frac{2}{d}\int_0^{d/2}\left|\underline{B}_\mathrm{y}(z)\right|^2\mathrm{d}z = \frac{\pi B_\mathrm{p}^2}{2|\underline{\mu}|}\frac{\mu''}{\mu'}\frac{\left(\lambda'+\lambda''\right)\sinh\left(\lambda'-\lambda''\right)+\left(\lambda'-\lambda''\right)\sin\left(\lambda'+\lambda''\right)}{\cosh\left(\lambda'-\lambda''\right)-\cos\left(\lambda'+\lambda''\right)}. \qquad \text{(A11)}$$

The difference between the calculated values provided by (A9) and (A11) will provide $W_\mathrm{cl,SIN}(f)$. Alternatively, $W_\mathrm{cl,SIN}(f)$ can be obtained by calculating the classical eddy current density as $\underline{j}_\mathrm{x}(z) = \mathrm{curl}(\underline{H}_\mathrm{y}(z)) = -(\partial\underline{H}_\mathrm{y}/\partial z)_\mathrm{x}$ and integrating it according to

$$W_{\mathrm{cl,SIN}}(B_{\mathrm{p}},f)=\frac{2}{d}\int_0^{d/2}\frac{1}{2\sigma f}\left|\frac{\mathrm{d}\underline{H}_y}{\mathrm{d}z}\right|^2\mathrm{d}z= \tag{A12}$$

$$=\frac{\pi}{2}\frac{{B_{\mathrm{P}}}^2}{\mu'}\cdot\frac{\left(\lambda'+\lambda''\right)\sinh\left(\lambda'-\lambda''\right)-\left(\lambda'-\lambda''\right)\sin\left(\lambda'+\lambda''\right)}{\cosh\left(\lambda'-\lambda''\right)-\cos\left(\lambda'+\lambda''\right)}$$